5736 *Inorg. Chem.* **2009**, *48*, 5736–5746
DOI: 10.1021/ic900632g

Inorganic Chemistry
Article

Synthesis and Nanoscale Characterization of $(NH_4)_4ThF_8$ and ThNF

G. W. Chinthaka Silva,[†] Charles B. Yeamans,[‡] Gary S. Cerefice,[†] Alfred P. Sattelberger,[§] and Kenneth R. Czerwinski*[,†]

[†]*Harry Reid Center for Environmental Studies, University of Nevada, Las Vegas, Box 454009, 4505 Maryland Parkway, Las Vegas, Nevada 89154,* [‡]*Department of Nuclear Engineering, University of California, Berkeley, 1140 Etcheverry Hall, M.C. 1730 Berkeley, California 94720-1730, and* [§]*Argonne National Laboratory, 9700 Cass Avenue, Bldg 221, Argonne, Illinois 60517*

Received November 28, 2008

Synthesis of $(NH_4)_4ThF_8$ by a solid state reaction of ThO_2 and NH_4HF_2 and the formation of ThNF by ammonolysis of $(NH_4)_4ThF_8$ and ThF_4 under different experimental conditions were investigated. The solid state reaction of ThO_2 with NH_4HF_2 led to the terminal product $(NH_4)_4ThF_8$ through a known intermediate $(NH_4)_3ThF_7$ and most likely two other unknown chemical phases as determined by X-ray powder diffraction. Conversion of $(NH_4)_4ThF_8$ into ThNF occurs through a ThF_4 intermediate phase. Studies on the ammonolysis of ThF_4 revealed it converted into ThNF through a continuous formation of low-stoichiometric thorium-nitride-fluorides such as $ThN_{0.79}F_{1.63}$ and $ThN_{0.9}F_{1.3}$. Thermal behavior of ThNF was also examined under different atmospheres and temperatures, with evaluation of formation kinetics. The ThNF decomposed to low-stoichiometric thorium nitride fluorides ($ThN_{x/3}F_{4-x}$) under different environments up to 1100 °C. Significant morphological changes in the products compared to that of the precursors confirmed the reaction steps involved. Microstructural characterization of $(NH_4)_4ThF_8$ and ThNF were performed by HRTEM and are presented in this work for the first time. The $(NH_4)_4ThF_8$ product was shown to contain polycrystalline characteristics in the majority of its nanostructure. On the other hand, ThNF has a high order of nanostructure, which explains the high thermal stability of the compound up to 1100 °C and the difficulty of making ThN_x, in initial target product, from the described experimental conditions.

1. Introduction

Actinide mononitrides and their mixed systems such as (U−Pu)N have been considered for advanced nuclear fuel applications.[1,2] They have excellent thermal, chemical, physical, and nuclear properties, with well-behaved mutual solubility properties, and are considered as a fuel material for the transmutation of minor actinides.[3] Thoria-based nitride fuels can also be considered in these different applications because of the analogous crystallography of thorium mononitride (ThN) to other nitride fuels such as UN. However, there is a very small amount of data reported on the thoria-based nitrides and related compounds. Microscopic characterizations on most of the thoria-based compounds such as oxides,[4] carbonates,[5] oxalates,[6] and hydrides[7] have been reported in literature. However, no such data can be found for thorium fluorides, nitrides, or nitride-fluorides. Lack of such substantial chemical data of these materials motivates their synthesis and characterization.

On the basis of previous studies performed on thorium nitrides (ThN_x), three common compounds can be identified. Those are ThN, Th_3N_4, [8,9] and Th_2N_3.[10,11] Synthesis of ThN_x involves heating of the thorium metal [12] or thorium hydride under ammonia or nitrogen atmosphere.[10,13] Reacting $ThCl_4$

*To whom correspondence should be addressed. E-mail czerwin2@unlv.nevada.edu. Phone: (702) 895 0501. Fax: (702) 895 3094.

(1) Matzke, Hj. *Advanced LMFBR Fuels*; Elsevier: Amsterdam, 1986; p 2.
(2) Takano, H.; Nishihara, K. *Prog. Nucl. Energy* **2002**, *40*, 473.
(3) Minato, K.; Akabori, M.; Takano, M.; Arai, Y.; Nakajima, K.; Itoth, A.; Ogawa, T. *J. Nucl. Mater.* **2003**, *320*, 18–24.
(4) Curran, G.; Sevestre, Y.; Rattray, W.; Allen, P.; Czerwinski, K. R. *J. Nucl. Mater.* **2003**, *323*, 41–48.
(5) Dash, S.; Singh, A.; Ajikumar, P. K.; Subramanian, H.; Rajalakshmi, M.; Tyagi, A. K.; Arora, A. K.; Narasimhan, S. V.; Raj, B. *J. Nucl. Mater.* **2002**, *303*, 156–168.
(6) Ananthasivan, K.; Anthonysamy, S.; Singh, S.; Rao, P. R. V. *J. Nucl. Mater.* **2002**, *306*, 1–9.
(7) Terrani, K. A.; Silva, G. W. C.; Yeamans, C. B.; Balooch, M.; Olander, D. R. *J. Nucl. Mater.*, accepted for publication.
(8) Benz, R.; Hoffman, C. G.; Rupert, G. N. *Phys. Inorg. Chem.* **1967**, *89*, 191–197.
(9) Auskern, A. B.; Aronson, S. *J. Phys. Chem. Solids* **1967**, *28*, 1069–1071.
(10) Olson, W. M.; Mulford, R. N. R. *J. Phys. Chem.* **1965**, *69*, 1223–1226.
(11) Aronson, S.; Auskern, A. B. *J. Phys. Chem.* **1966**, *70*, 3937–3941.
(12) Chiotti, P. *J. Am. Ceram. Soc.* **1952**, *35*, 123–130.
(13) Uno, M.; Katsura, M.; Miyake, M. *J. Less-Common Met.* **1986**, *121*, 615–619.

Published on Web 06/11/2009

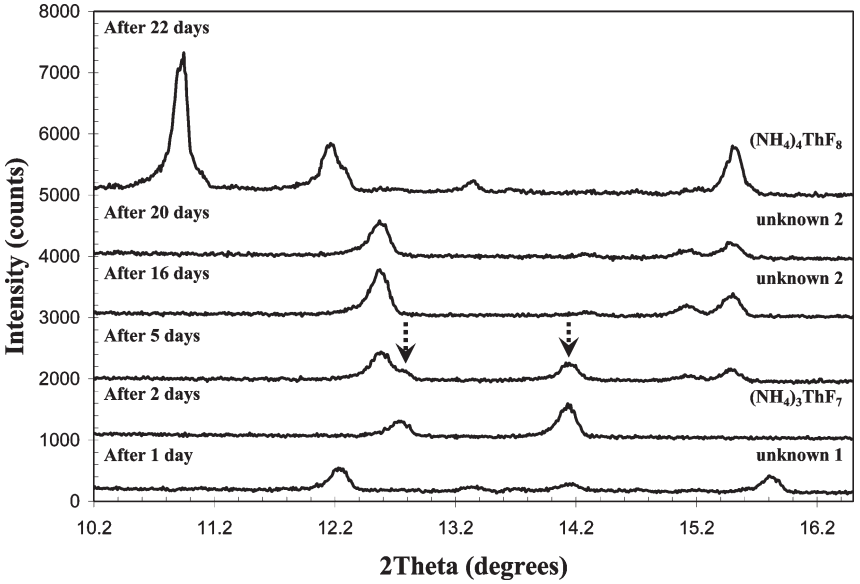

Figure 1. XRD patterns indicating the reaction progress of the 100 mg batch of ThO_2 mixed with excess NH_4HF_2. Only a part of the XRD patterns are shown for clarity of the comparison.

with $LiNH_2$ in liquid ammonia and then heating under nitrogen gas is another way to synthesize the thorium nitrides.[15] In most of these methods, thorium mononitride is made by thermally decomposing higher nitrides such as Th_3N_4 at 1500 °C under inert atmosphere.[8,10,16] However, synthesis of ThN_x with high phase purity is difficult because of secondary ThO_2 formation. In particular, the ThN produced by these methods shows the presence of ThO_2 chemical phase as it is highly susceptible to oxidation.[13] This fact complicates the synthesis of ThN_x using above-mentioned high-temperature routes.

Therefore, a low-temperature fluoride route based on a recent research work on synthesizing UN [14] was investigated to make thorium nitrides and related compounds in this work. In this method, ThO_2(s) was reacted with excess (4.2 molar) NH_4HF_2(s) to make ammonium thorium fluoride $\{(NH_4)_xThF_{x+4}\}$ which was then used as the precursor for making the desired nitrides. Heat treatment of $(NH_4)_xThF_{x+4}$ under NH_3(g)/ammonolysis and further heating of any higher nitrides formed under Ar(g) was envisaged in the subsequent steps. Nevertheless, the expected ThN_x compounds were not observed, and instead ThNF was obtained as the terminal product up to a temperature of 1100 °C. Similar reactions and product formations have also been reported by different groups.[16]

The product of the reaction between ThO_2(s) and ammonium hydrogen fluoride (NH_4HF_2(s)) was reported as $(NH_4)_4ThF_8$.[17] Penneman et al.[18] as well as Glavic et al.[19] synthesized the same ammonium thorium fluoride compound by reacting ThF_4 with an aqueous ammonium fluoride solution. In the current work, the same $(NH_4)_4ThF_8$ is reported as the terminal product of the ThO_2(s) reaction with NH_4HF_2(s) but with an intermediate $(NH_4)_3ThF_7$(s) phase. Two more possible intermediate chemical phases with different stabilities with respect to reaction kinetics are also discussed. Ammonolysis of $(NH_4)_4ThF_8$ produced ThNF. In this process ThF_4 was also identified as an intermediate phase before forming ThNF. In the literature, Juza et al.[20] reported ThNF formation by heating ThF_4 at 850 °C under flowing ammonia gas confirming what was found in the current work. However, a systematic study on these systems cannot be found in literature. Therefore, the products observed when using different temperatures in the ammonolysis step of $(NH_4)_4ThF_8$ and ThF_4 and a complete study on the thermal behavior of ThNF up to 1100 °C under high-purity atmospheres of Ar(g) and N_2(g) are presented here. On the basis of the results of these experiments, a possible reaction mechanism for the formation of ThNF from $(NH_4)_4ThF_8/ThF_4$ under ammonia gas is also proposed. Microscopy was used for the first time to characterize the morphology and nanostructures of these thorium compounds. These observations were further used in explaining the formation of different products at separate reaction steps.

2. Experimental Details

2.1. Synthesis of Ammonium Thorium Fluoride. A solid state reaction was utilized in synthesizing ammonium thorium fluorides. Two batches of ThO_2 (100 mg and 1000 mg) were used in this experiment. The ThO_2 (STREM Chemicals, 99.99%) powder was added into a polyethylene vial with ground NH_4HF_2 (Fisher Scientific, 99.99%) in a 1:4 molar ratio with 10 mol. % excess NH_4HF_2. The sample was then mixed with a spatula for 10 min. The reaction was allowed to progress in the closed vial at room temperature until completion. Reaction progress was evaluated by periodically removing a small sample for X-ray diffraction analysis.

2.2. Ammonolysis of $(NH_4)_4ThF_8$ and Heating of ThNF. The resulting $(NH_4)_4ThF_8$ product was placed on a platinum sheet

(14) Yeamans, C. B.; Silva, G. W. C.; Cerefice, G. S.; Czerwinski, K. R.; Hartmann, T.; Burrell, A. K.; Sattelberger, A. P. *J. Nucl. Mater.* **2008**, *374*, 75–78.
(15) Brese, N. E.; Disalvo, F. J. *J. Solid State Chem.* **1995**, *120*, 378–380.
(16) Aronson, S.; Cisney, E.; Gingerich, K. A. *J. Am. Ceram. Soc.* **1967**, *50*, 248–252.
(17) Wani, B. N.; Patwe, S. J.; Rao, U. R. K.; Venkateswarlu, K. S. *J. Fluorine Chem.* **1989**, *44*, 177–185.
(18) Penneman, R. A.; Ryan, R. R.; Rosenzweig, A. *Chem. Commun.* **1968**, *16*, 990–991.
(19) Glavic, P.; Slivnik, J.; Bole, A. *J. Inorg. Nucl. Chem.* **1973**, *35*, 427–432.
(20) Juza, R.; Sievers, R. *Z. Anorg. Allg. Chem.* **1968**, *363*, 258–272.

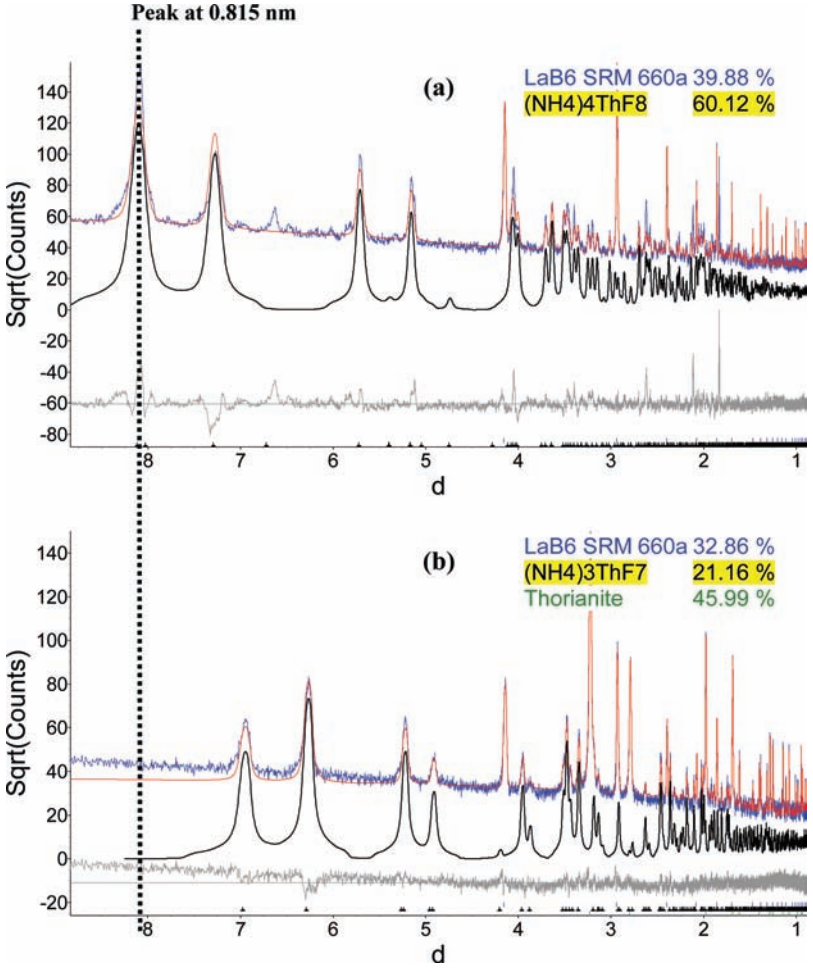

Figure 2. Observed and the calculated XRD powder patterns of (a) $(NH_4)_4ThF_8$ and (b) $(NH_4)_3ThF_7$ samples. Calculated and the observed patterns are shown in continuous and scattered lines, respectively. Calculated patterns of both $(NH_4)_4ThF_8$ and $(NH_4)_3ThF_7$ are highlighted in the corresponding figures. X-axes are in 10^{-1} nm units. Square root of counts was used as the scale of Y-axis for proper display of the calculated patterns. Allowed line positions for the separate phases are marked as vertical lines at the bottom with arrows for the highlighted pattern.

and inserted into a 25 mm diameter quartz-glass tube. The tube was closed on either end with a 25 mm quartz Solv-Seal (Andrews Glass Co., Inc.), and sealed using Pyrex Solv-Seal caps fitted with 15 mm high vacuum Teflon stopcocks. Ammonia gas (high-purity 99.999%, Praxair) was flushed through the tube for 5 min to pre-equilibrate and purge the system. The system was heated to 800 °C under a constant flow of ammonia gas at 1 atm. The gas flow was constant throughout the experiment. Total heating time was varied up to 5 h and then cooled to room temperature. Once the samples cooled, the ammonia gas flow was terminated and the product was removed for analysis. The reaction was also performed at 1000 °C for 45 min and at 1100 °C for 15 min. All heating of the products were performed with high-purity (99.999%) Ar, Ar/H_2 (5%), N_2, and N_2/H_2 (5%). A zirconium metal sponge was used as an oxygen getter in experiments at 1100 °C.

2.3. Characterization Methods. 2.3.1. X-ray Powder Diffraction (XRD). XRD was used to identify phase distributions of the synthesized samples using a Philips PANalytical X'Pert Pro instrument with a Cu Kα radiation and a Ni filter. Lattice parameter refinements and phase quantifications were done using TOPAS software.[21] TOPAS was designed to analyze powder data and uses the Rietveld method to fit the calculated patterns to observed patterns. With TOPAS, structure determination does not include any methods that require integrated intensity extraction as it is performed in direct space using step intensity data. Structure determination is made in TOPAS by initially estimating the cell parameters of the structure, using a rough knowledge about the cell content, and speculating the space group of the structure. Initial deduction of the structure was done using ICSD (Inorganic Crystal Structure Database) reference patterns as the models for the refinement. The ICSD XRD pattern numbers 9889 and 14128 were used for $(NH_4)_4ThF_8$ and $(NH_4)_3ThF_7$, respectively. For ThO_2 and ThNF, the ICSD XRD pattern numbers 61586 and 35745 were used, respectively. LaB_6 SRM (Standard reference Material) 660a was used as the internal standard for accurate lattice parameter refinements.

Electron density map of ThNF was also used to confirm the crystallography and to support the HRTEM findings. Le Bail decomposition[22] was used to extract the individual observed structure factor amplitudes (F_{obs}) of the XRD powder pattern using Jana2000.[23] These observed structure factors were then used to calculate the electron density maps of the compound by the charge-flipping algorithm using Superflip program.[24] The calculated electron density maps were visualized using UCSF Chimera.[25]

(21) Coelho, A. A. *J. Appl. Crystallogr.* **2000**, *33*, 899–908.

(22) Bail, A.; Duroy, H.; Fourquet, J. L. *Mater. Res. Bull.* **1998**, *23*, 447–452.

(23) DusÏek, M.; PetrÏõÂcÏek, V.; Wunschel, M.; Dinnebier, R. E.; Smaalen, S. *J. Appl. Crystallogr.* **2001**, *34*, 398–404.

(24) Palatinus, L.; Chapuis, G. *J. Appl. Crystallogr.* **2007**, *40*, 786–790.

(25) Pettersen, E. F.; Goddard, T. D.; Huang, C. C.; Couch, G. S.; Greenblatt, D. M.; Meng, E. C.; Ferrin, T. E. *J. Comput. Chem.* **2004**, *25*(13), 1605–1612.

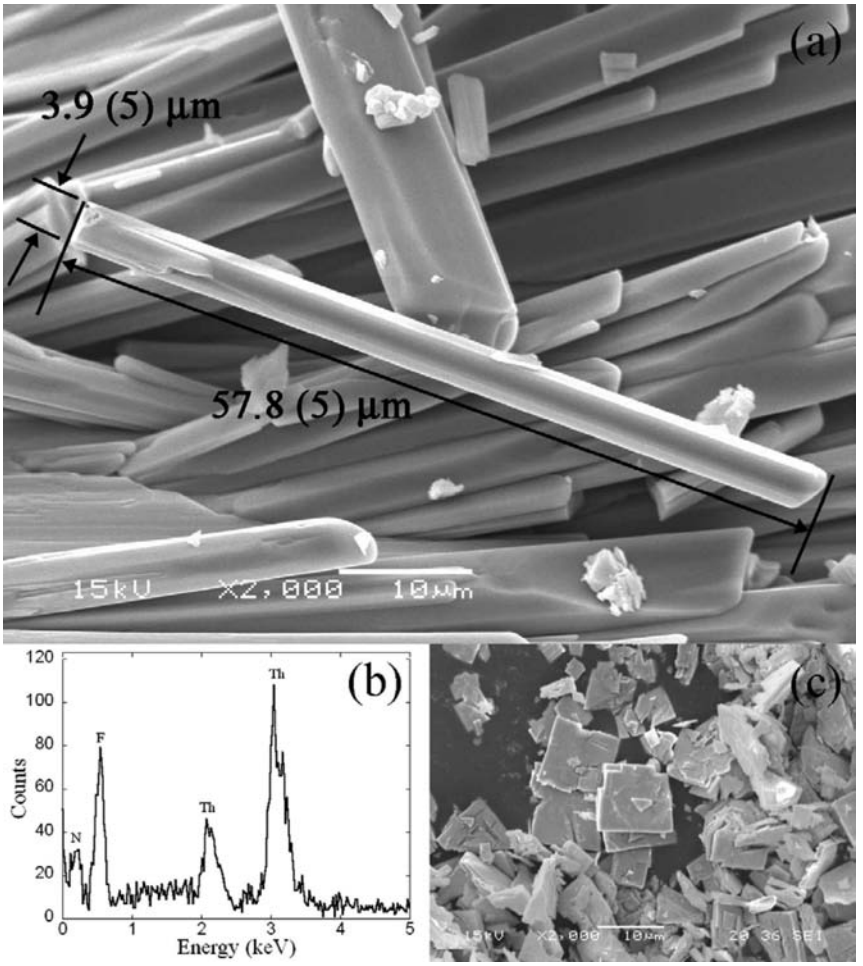

Figure 3. Secondary-electron SEM image (a) and the corresponding EDS spectrum (b) of the synthesized $(NH_4)_4ThF_8$ and the SEM image of ThO_2 (c).

2.3.2. Microscopy. Morphological studies of the samples were done using scanning electron microscopy (SEM) and transmission electron microscopy (TEM). SEM imaging was performed using a JEOL scanning electron microscope model JSM-5610 equipped with secondary electron (SE) and backscattered electron (BE) detectors and an Oxford ISIS EDS (energy dispersive spectroscopy) system. The acceleration voltage used in SEM was 15 kV. TEM was performed using TECNAI-G2-F30 with a 300 keV field emission gun. All TEM images were recorded using a slow scan CCD camera attached with a Gatan GIF 2000 image filter. The conventional bright field (BF) diffraction contrast mode and the high resolution (HR) TEM modes coupled with selected area electron diffraction (SAED) patterns and Fast Fourier Transformation (FFT) micrographs were utilized to characterize the samples. X-ray energy dispersive spectrometry (XEDS) was used to determine the elemental distributions. Further description of the sample preparation techniques used for this work can be found in Silva et al. [26]. The thorium samples for TEM analysis were prepared by the solution-drop method and microtome cutting. In the solution drop method, the samples were ground to microsize in a mortar and mixed with ethanol. One drop of the solution was added onto a 3 mm diameter carbon film supported on a copper grid that was used as the sample holder. A Leica EM UC6rt microtome was used for sample cutting of 25 to 75 nm thicknesses. More details of these sample preparations are discussed in Silva et al.[26]

(26) Silva, G. W. C.; Yeamans, C. B.; Ma, L.; Cerefice, G. S.; Czerwinski, K. R.; Sattelberger, A. P. *Chem. Mater.* **2008**, *20*, 3076–3084.

3. Results

3.1. Formation and Characterization of $(NH_4)_4ThF_8$. The XRD patterns of the samples showed that the terminal product of the reaction of NH_4HF_2 with ThO_2 is $(NH_4)_4ThF_8$ with a triclinic unit cell and $P\bar{1}$ space group. Further analysis confirmed the formation of an intermediate $(NH_4)_3ThF_7$ chemical phase of an orthorhombic unit cell and *Pnma* space group in the reaction. Figure 1 is a graphical view of the kinetics of ThO_2 (100 mg batch) solid state reaction with NH_4HF_2 at room temperature. After 1 day of mixing the two reactants, a new chemical phase was formed according to the XRD pattern in Figure 1. This XRD pattern has some similarities to the pattern of the terminal $(NH_4)_4ThF_8$ chemical phase even though refinement assuming similar crystallography was not successful. The intermediate chemical phase which was identified as $(NH_4)_3ThF_7$ was formed after 2 days. The XRD pattern of the sample after 5 days displays some of the peaks that correspond to $(NH_4)_3ThF_7$ as indicated by arrows. These peaks start to diminish with the formation of new set of peaks at 2θ values of 12.6, 15.1, and 15.5°. The XRD pattern formed with these peaks was prominent and was believed to be another intermediate phase that was not identifiable as the known ammonium fluorides of thorium or any other actinides such as uranium and neptunium. This new and unknown chemical phase remained until it completely

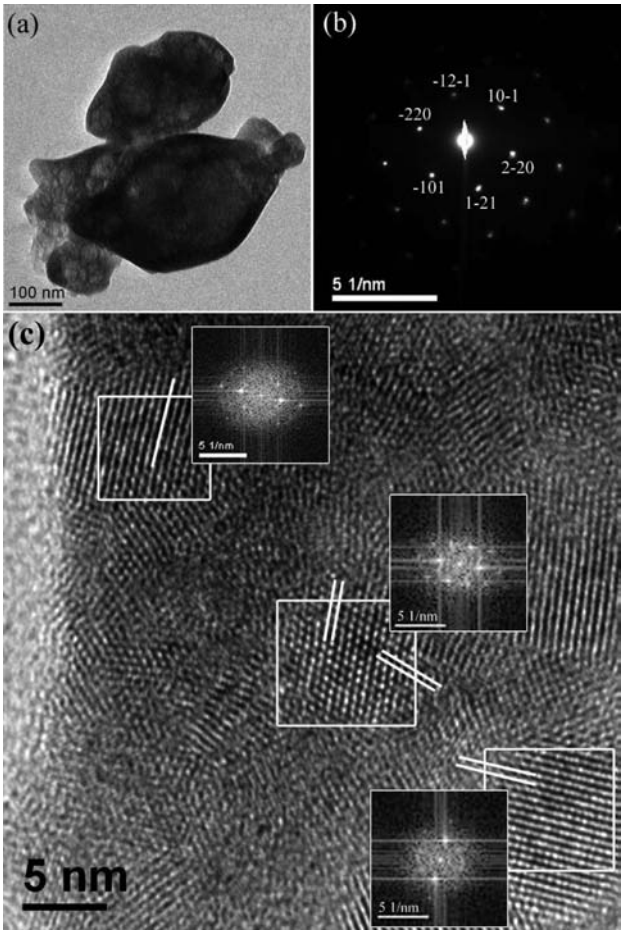

Figure 4. (a) TEM BF image, (b) [111] electron diffraction pattern, and (c) HRTEM image of $(NH_4)_4ThF_8$ ground particle.

changed into the terminal $(NH_4)_4ThF_8$ chemical phase after 22 days.

Wani et al.[13] describe the reaction of solid ThO_2 with solid NH_4HF_2 at room temperature to be quick (2 h) in forming $(NH_4)_4ThF_8$. However, they reported an absence of the reflection at $d = 0.815$ nm in the XRD pattern of this product. Furthermore, they did not identify or matched their XRD pattern to $(NH_4)_3ThF_7$ which has some similar reflections to that of $(NH_4)_4ThF_8$ with the absence of the peak at $d = 0.815$ nm (Figure 2). The chemical phase they were describing can also be due to the first unknown XRD pattern that was described earlier in Figure 1 (XRD pattern after 1 day). Further comparison with this is difficult as the experimental parameters such as reactant mass or XRD patterns of the products are not reported.

The observed and the calculated XRD patterns of $(NH_4)_4ThF_8$ and a sample containing $(NH_4)_3ThF_7$ are shown in Figure 2, panels a and b, respectively. The patterns of both $(NH_4)_4ThF_8$ and $(NH_4)_3ThF_7$ matched well with the reference patterns in the ICSD of numbers 9889 and 14128, respectively. Few impurity peaks in both samples were identified, especially near 0.68 nm *d*-spacing value in the $(NH_4)_4ThF_8$ sample. These impurity peaks together with the amorphous characteristics of the samples can be accounted for by the excess NH_4F/NH_4HF_2 salts. The refined triclinic unit cell parameters of $(NH_4)_4ThF_8$ compound are $a = 0.85041$ (7), $b = 0.83667$ (7), and $c = 0.73372$ (6) nm. Lattice parameters of orthorhombic $(NH_4)_3ThF_7$ with a space group of *Pnma* were refined to be $a = 0.3952(9)$, $b = 0.7932(5)$, and $c = 0.70462(5)$ nm.

The secondary electron SEM image of the $(NH_4)_4ThF_8$ sample (Figure 3a) indicates well-crystallized sample particles with an acicular shape (Figure 3a) compared to the plate-like shape of the reactant, ThO_2, (Figure 3c). Furthermore, the acicular crystals that Penneman et al.[18] described can also be clearly seen in this figure. The elemental distribution of the $(NH_4)_4ThF_8$ sample obtained using the EDS (Figure 3b) also shows the presence of the expected components in the sample.

TEM BF image of the $(NH_4)_4ThF_8$ particles from a ground sample is shown (Figure 4a). The SAED pattern in Figure 4b was obtained by focusing on an area of the large particle seen in the bottom half of Figure 4a, and this pattern is in [111] zone axis. Figure 4c is a HRTEM image of the same particle displaying lattice fringes in several different orientations as indicated in the image. Some of these domains have high point resolution in two directions while others exhibit either one or no directional fringe properties. This observation suggests that the $(NH_4)_4ThF_8$ obtained is a polycrystalline material.

On the other hand, Figure 5b shows a well-oriented set of lattice fringes of $(NH_4)_4ThF_8$ corresponding to the (1−11) lattice plane distributed in a larger area than in the nanocrystalline areas found in Figure 4c. This set of lattice fringes are also disturbed by another similar-sized nanoparticle domain, as indicated by the arrow, which has being grown from the other side of the particle. This feature further implies a polycrystalline characteristic of the sample even though this area consists of comparatively large nanoparticles.

3.2. Synthesis and Characterization of ThNF. Ammonolysis of $(NH_4)_4ThF_8$ or the heat-treatment of the sample under ammonia atmosphere at three different temperatures (Table 1) showed that the final product of this second reaction step is ThNF. At 800 °C, 300 min were required to synthesize this terminal product. Increasing the reaction temperature resulted in a significant decrease in reaction time, with sample heating at 1100 °C for 15 min optimal for synthesis of ThNF. The elemental analysis of this sample determined by EDS is shown in Table 2. The Th/N/F molar ratio of the compound is approximately 1:1:0.6. On the basis of the error associated with the EDS on quantification and as EDS is considered a semiquantitative method, the stoichiometry of the compound can be considered close to 1:1:1 (ThNF). In the sample heated for 300 min at 800 °C, a secondary ThO_2 phase was identified because of prolonged exposure to minute oxygen impurities in the system.

The XRD pattern of the ThNF sample synthesized by ammonolysis of $(NH_4)_4ThF_8$ at 1100 °C for 15 min (Figure 6) confirms the sample is single-phased. The refined lattice parameter of the rhombohedral unit cell was 0.71312 (5) nm which agrees well with the literature value of 0.7130 (3) nm.[20] The phase density of ThNF was calculated to be 9.369 (2) g/cm^3.

The secondary SEM image of a ThNF sample (Figure 7a) shows plate-like particle shapes. The 15,000 times magnified SEM image (Figure 7b) further displays pitted and porous characteristics of the ThNF particle

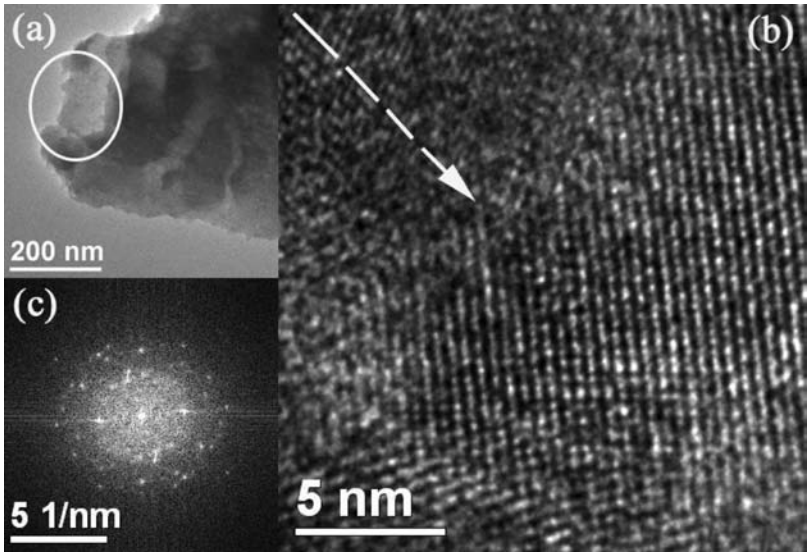

Figure 5. (a) TEM BF image of a ground $(NH_4)_4ThF_8$ particle. (b) The HRTEM image of the circled area of (a) and (c) the corresponding FFT.

Table 1. Temperature Effect on the Ammonolysis of $(NH_4)_4ThF_8$

		product			
temperature/ °C	time/ min	primary phase	weight %	secondary phase	weight %
800	300	ThNF	79.0(6)	ThO_2	21.0(6)
1000	45	ThNF	100		
1100	15	ThNF	100		

Table 2. Elemental Analysis of the As-Synthesized ThNF by EDS

element	averaged atom percentages (%)
N K (±1.25)	39.0
F K (±1.26)	21.6
Th K (±1.47)	39.4
Th/N/F molar ratio	1:0.99:0.60

surface. Furthermore, the corresponding EDS spectrum (Figure 7c) of this sample confirms the presence of thorium, fluorine, and nitrogen. The nitrogen peak partially overlaps with the background peak from carbon tape that was used to mount the sample. SEM image of ThF_4 is also shown in Figure 7d for the comparison purposes.

A 50 nm thick sample of ThNF was microtome cut for TEM imaging. Figure 8a shows a low-resolution TEM BF image of few ThNF particles thus prepared. As microtome cutting was applied for the specimen preparation, the cross-sectional view of the sample at HRTEM is supposed to show a uniform intensity across a focused area. However, most of the areas investigated showed intensity variance of the images at high-resolution. HRTEM of one such area is shown in Figure 8b. The area in this image shows a continuous set of ThNF lattice fringes corresponding to (0−11) planes under [100] beam. Most of the area displays lattice fringes only in one direction except for some lattice fringes in the area depicted by B−C. A line scan across the image on a randomly selected lattice fringe from A through D (Figure 8d) shows that the intensity of the image changes considerably. The intensities from A to B do not vary much, but it is at highest in the region denoted by B−C. From C to D, the intensities start to change abruptly and approach a minimum at the end of the line. This observation suggests a thickness variance across the scanned area forming a thinner region of about 6 nm, given the length of the line scanned to be 36 nm. The void spaces of the ThNF particles detected by SEM imaging were 50 to 200 nm in width. This implies a continuation of void spaces down to nanoscale of the ThNF compound.

HRTEM of another area of the same particle in Figure 8a is displayed in Figure 9. Two rectangle areas of Figure 9 were enlarged using a smooth spatial filter to obtain HRTEM images in Figure 9b and Figure 10. The beam direction of these HRTEM images is [110]. Lattice fringes in Figure 9b provide a width of 0.265 nm for a single layer of fringes corresponding to a reflection plane of (221). Intensity difference between areas A and B reveals more intuitive structural detail of ThNF as depicted in Figure 10. Thickness variance as identified previously is the probable reason for such a difference in intensities of two areas within 30 nm. Lattice fringes in area B as shown in Figure 10 provide more detail than area A. Spacing between two layers of lattice fringes in Figure 10 is 0.225 nm, which is close to the *d*-spacing of (333) lattice plane of ThNF. Furthermore, this spacing is less than the width of a single layer of lattice fringes in area A (0.265 nm) demonstrating a shift in the atomic planes that create the lattice fringes in the HRTEM images. The electron density map of ThNF calculated from XRD pattern utilizing charge flipping, which is the inset to the upper right of Figure 10, also confirms the structural details observed with HRTEM imaging. As the electron density map indicates a high electron density at

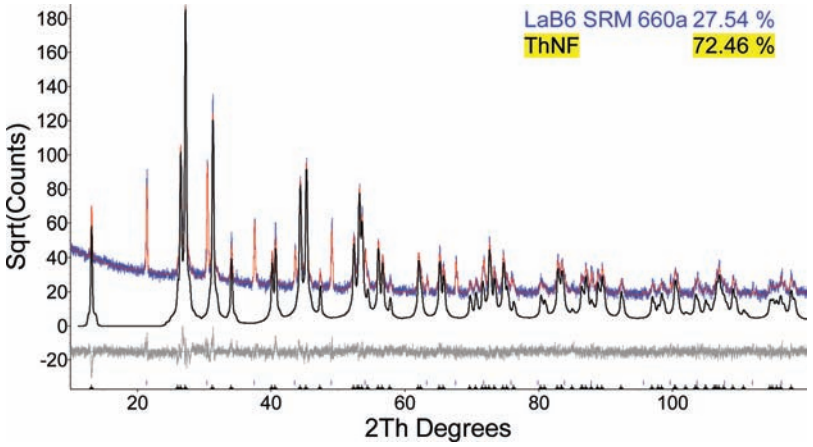

Figure 6. Observed (top continuous line) and calculated (highlighted continuous line for ThNF) patterns of ThNF synthesized by heating $(NH_4)_4ThF_8$ at 1100 °C for 15 min under NH_3. Square root of counts was used as the scale of *Y*-axis for proper display of the calculated patterns.

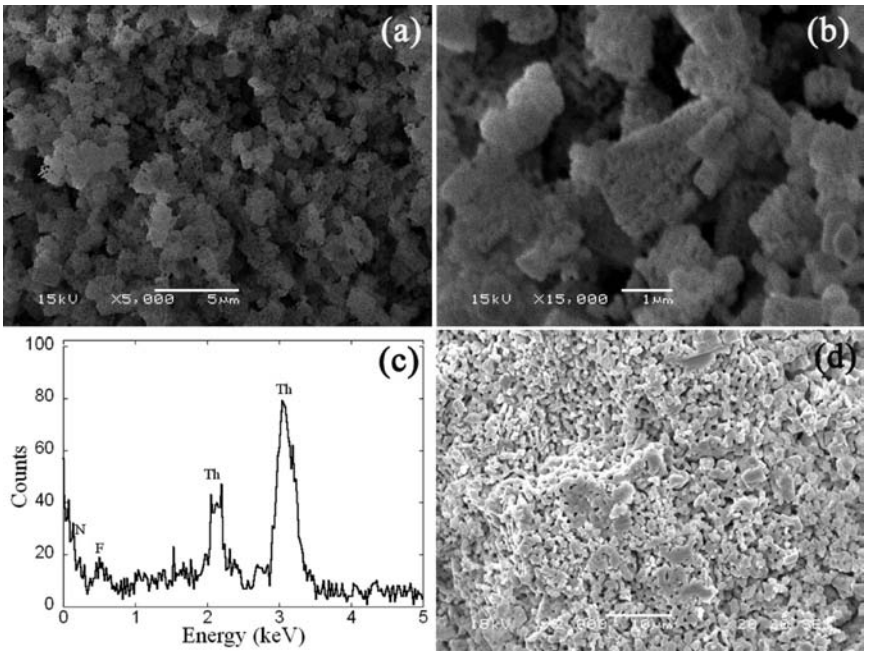

Figure 7. Secondary electron SEM images of the ThNF sample, (a) showing the morphology at ×5,000 magnification and (b) at ×15,000 magnification, (c) the corresponding EDS spectrum of ThNF, (d) and the SEM image of ThF_4.

locations where Th atoms reside within the crystal structure of ThNF, the HRTEM imaging will only show the intensities due to Th atoms. Repetition of such structural units will give a well-ordered nanostructure (Figure 10). Atomic resolution of the hexagonal-like order of atoms in the HRTEM image is different from point-to-point as indicated by circles in the image. The atomic planes in (111) direction of the packed rhombohedral unit cells are in and out of plane slightly such that the depth of the imaging can change as indicated in the inset of the Figure 10 (lower to the electron density map). All these observations confirm the presence of single-phased ThNF in the sample.

3.3. Ammonolysis of ThF_4 and the Thermal Behavior of ThNF. Heating of the $(NH_4)_4ThF_8$ sample at 800 °C for 60 min formed ThF_4 in agreement with Wani et al.[17] The observed XRD powder pattern together with the calculated pattern of ThF_4 chemical phase identified is shown (Figure 11). The lattice parameters, $a = 1.3049$ (3), $b = 1.1120$ (2), $c = 0.8538$ (2) nm[27] for the monoclinic-ThF_4 agree fairly well with the refined lattice parameters of the measured pattern, $a = 1.30444$ (7), $b = 1.10118$ (6), $c = 0.85343$ (5) nm.

After identifying ThF_4 as an intermediate in the conversion of $(NH_4)_4ThF_8$ to ThNF, ThF_4 was heated under varying experimental conditions (Table 3) to determine the reaction mechanism. Removal of fluorine atoms from the ThF_4 and incorporation of nitrogen to fill those vacant sites can be observed as the low-stoichiometric chemical phases of thorium nitride fluorides begin to appear in the samples (Table 3). Figure 12 shows the XRD powder pattern refinement of the $ThN_{0.79}F_{1.63}$ sample, which was synthesized by heating ThF_4 at 800 °C for 60 min. Treating ThF_4 for 300 min under NH_3(g)

(27) Benner, G.; Muller, B. G. *Z. Anorg. Allg. Chem.* **1990**, *588*, 32–42.

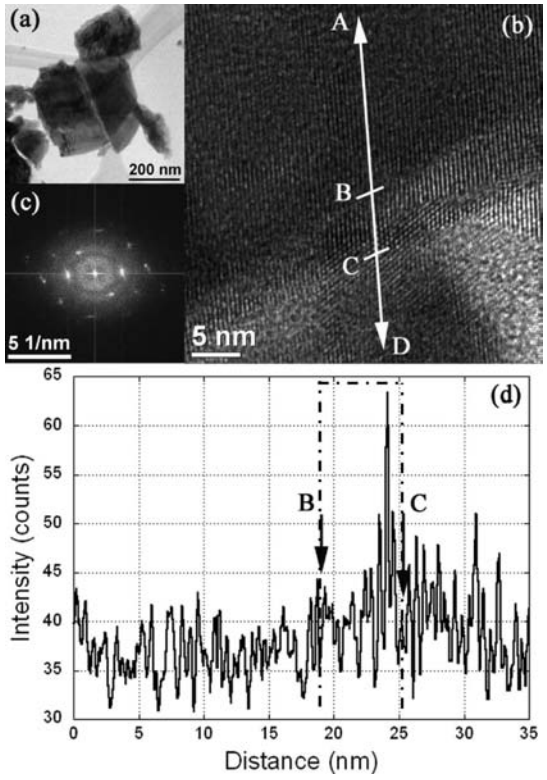

Figure 8. TEM BF of a microtome cut ThNF sample, (b) HRTEM image, (c) FFT of HRTEM, and (d) experimental intensity profile along A−B in HRTEM.

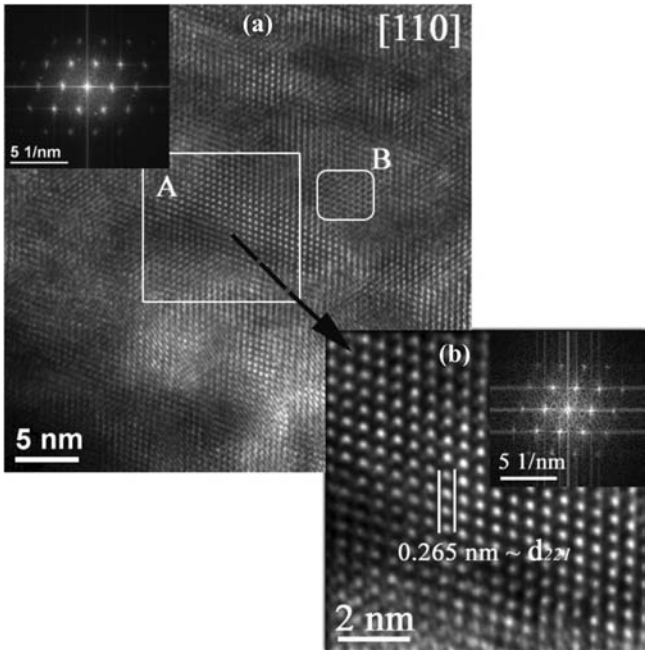

Figure 9. (a) HRTEM of another area of the particle in Figure 8a. (b) Enlarged image of the area denoted by letter A with a rectangle. The area B denoted by a rounded rectangle is used in Figure 10. Onsets of each image are the corresponding FFT micrographs.

further reduced the fluorine content from the reactant producing ThNF (79 wt %) along with $ThN_{0.79}F_{1.63}$ (21 wt %). XRD powder refinement of this sample is displayed in Figure 13 with highlighting the calculated pattern for $ThN_{0.79}F_{1.63}$. A complete formation of ThNF

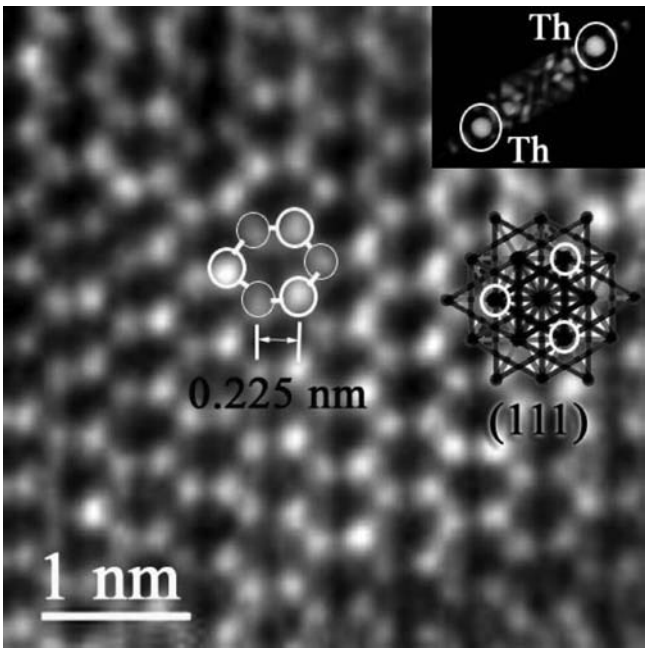

Figure 10. HRTEM of the particle area denoted by letter B in Figure 9. Inset to the upper right side is the electron density map calculated by ThNF XRD pattern using charge flipping. A model of the molecule in (111) direction is also inserted.

was observed after 600 min with no ThO_2 impurities (Figure 14a). However, a 17.6(7) wt % ThO_2 secondary phase was detected on heating ThF_4 at 1000 °C for 75 min (Figure 14b) whereas a 45 min heating did not show any impurity phase. These three observations suggest that prolonged heating at elevated temperatures form a ThO_2 secondary chemical phase because of the oxygen partial pressure produced by the quartz furnace tube used in the experiment.

Thermal stability of ThNF under different atmospheres was evaluated and the results summarized (Table 4). Using high-purity argon (99.999%) at 1100 °C, ThNF decomposes into $ThN_{0.79}F_{1.63}$ with a formation of secondary ThO_2 phase probably because of minor oxygen impurities formed in the experimental setup at this temperature. Under N_2 and N_2-H_2 (5%) environments, ThNF decomposed into another, similar low-stoichiometric thorium-nitride-fluoride ($ThN_{0.90}F_{1.30}$).

4. Discussion

The terminal product of ThO_2(s) reaction with NH_4HF_2(s) at ambient conditions was $(NH_4)ThF_8$, as previously reported.[17] This work determined the reaction proceeds through a known intermediate chemical phase $(NH_4)_3ThF_7$(s) that was formed after less than 2 days of mixing ThO_2 with NH_4HF_2. Two other possible phases of unknown chemical compositions were also intermediates in the reaction. Further interaction of the remaining ThO_2 with NH_4HF_2/NH_4F and the transformation of $(NH_4)_3ThF_7$ into the terminal $(NH_4)_4ThF_8$ took up to 22 days for a sample mass of 100 mg and 60 days for a sample mass of 1000 mg. Wani et al. reported [17] that $(NH_4)ThF_8$ to be formed after 2 h based on the XRD pattern obtained for the sample. However, the sample size was not reported. A sample under 100 mg could react to completion within a few hours. The XRD pattern in the previous work did not include the peak near $d = 0.815$ nm

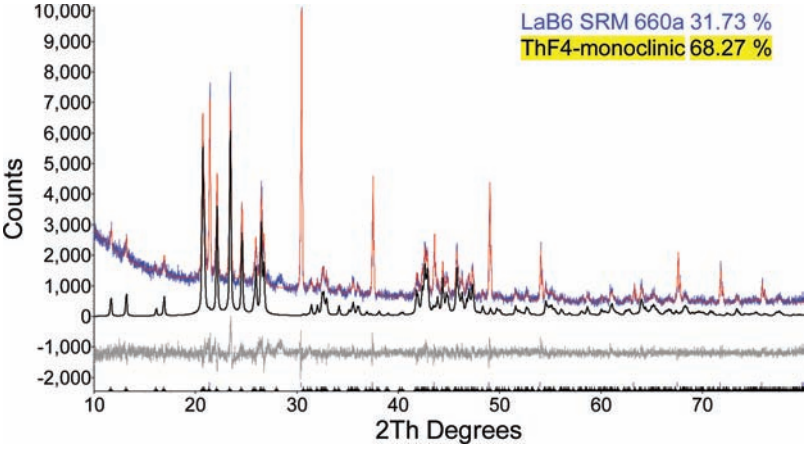

Figure 11. XRD powder pattern of the sample synthesized by heating $(NH_4)_4ThF_8$ at 800 °C for 60 min under NH_3(g). The calculated pattern of ThF_4 is highlighted.

Table 3. Ammonolysis of ThF_4

		product			
temp./ °C	time/ min	primary phase	mass %	secondary phase	mass %
800	60	$ThN_{0.79}F_{1.63}$	73.6(2)	unreacted ThF_4	26.4(2)
800	240	ThNF	79.0 (1)	$ThN_{0.9}F_{1.3}$	21.0 (1)
800	300	ThNF	79.0(6)	$ThN_{0.9}F_{1.3}$	21.0(6)
800	600	ThNF	100		
1000	45	ThNF	100		
1000	75	ThNF	82.4 (6)	ThO_2	17.6 (7)
1100	15	ThNF	100		

which could probably differentiate chemical composition of the sample to be $(NH_4)_3ThF_7$ or $(NH_4)_4ThF_8$. Observation of another chemical composition could also be possible according to the XRD patterns identified for two unknown chemical phases as indicated in Figure 1. In this current work, it was found that $(NH_4)_3ThF_7$ forms within 2 days of mixing ThO_2 and $(NH_4)_2HF_2$ whereas $(NH_4)_4ThF_8$ takes up to months depending on the sample size.

Ammonolysis of $(NH_4)_4ThF_8$ at 800 °C produced ThNF through ThF_4. Therefore, further studies of the thorium system were performed using ThF_4. Heat treatment of ThF_4 under NH_3 at different temperatures demonstrated a ThF_4 decomposition through removing some of the fluorine atoms in the crystal system. Nitrogen incorporates into those vacant cites of the ThF_{4-x}, resulting in new phases with the chemical formula of $ThN_{x/3}F_{4-x}$, occurred because of the nitrogen pressure in the cover gas. Removal of fluorine and the incorporation of nitrogen to those vacancies seized after the Th/N/F molar ratio of $ThN_{x/3}F_{4-x}$ chemical phases reached 1:1:1, forming ThNF as the terminal product. Further heating of ThNF up to 1100 °C under ammonia and other atmospheres examined in this work resulted only in the formation of low-stoichiometric thorium nitride fluorides and an impurity phase ThO_2 because of minor oxygen pressure coming from the quartz tubing used in the experiment at elevated temperatures. Experiments performed at

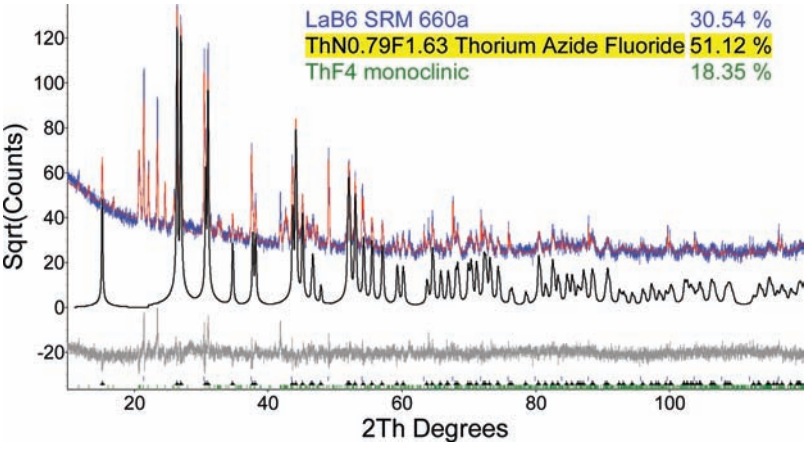

Figure 12. XRD powder refinement of the ThF_4 sample after the ammonolysis at 800 °C for 1 h. The calculated pattern of $ThN_{0.79}F_{1.63}$ is highlighted. Square root of counts was used as the scale of *Y*-axis for proper display of the calculated patterns.

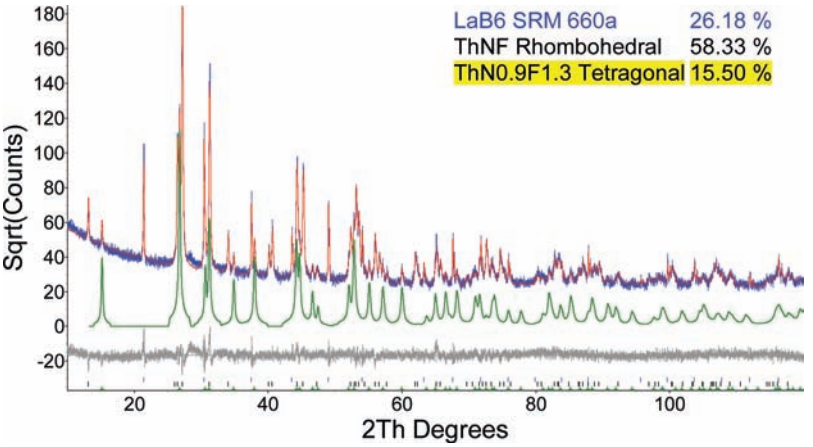

Figure 13. Calculated and observed XRD patterns of ThF_4 after the ammonolysis at 800 °C 300 min.

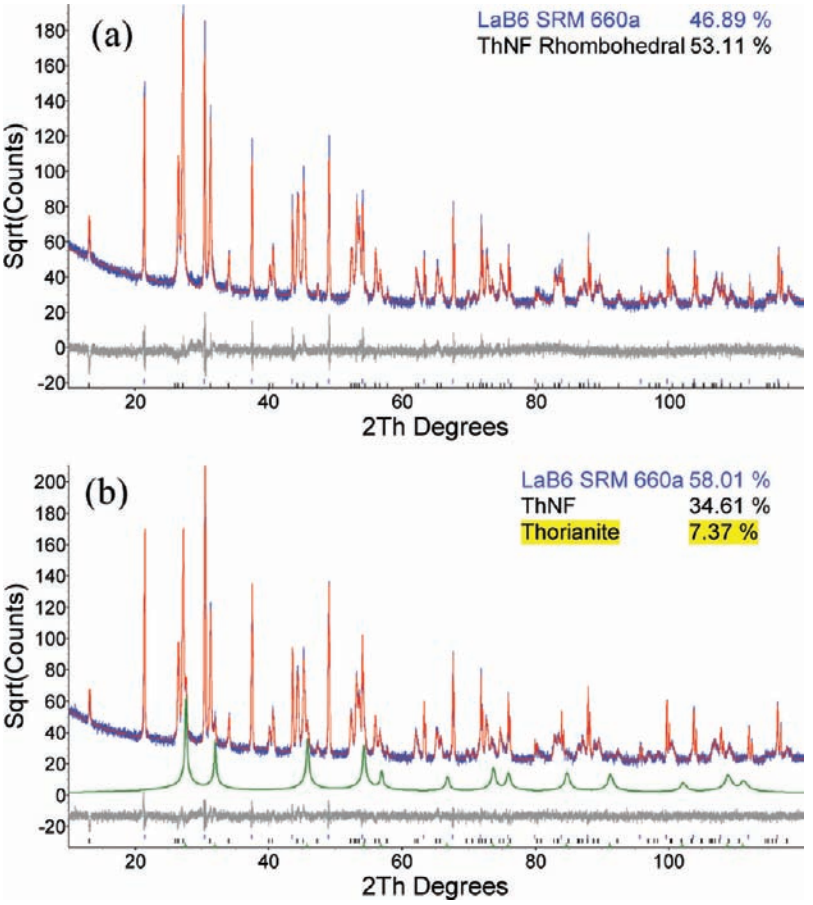

Figure 14. XRD powder refinements of ThF_4 after the ammonolysis at 800 °C for 600 min (a) and at 1000 °C for 75 min (b).

Table 4. Thermal Behavior of ThNF under Different Atmospheric Conditions

atmosphere	temperature/ °C	time/ min	product	secondary phases
Ar	1100	60	$ThN_{0.79}F_{1.63}$	ThO_2
$Ar-H_2$ (5%)	1100	60	ThO_2	
N_2	1100	60	$Th0_{0.90}F_{1.30}$	ThNF, ThO_2
N_2-H_2 (5%)	1100	60	$ThN_{0.90}F_{1.30}$	ThO_2
N_2-H_2 (5%)	1100	120	ThO_2	

different temperatures and heating times using same cover gas (Figure 14) suggest this observation confirming that the cover gases were high purity (99.999%) as purchased. Although variation of the experimental conditions impacted the stoichiometry of ThNF, no conditions yielded a pure thorium nitride (ThN_x) phase under these experimental

conditions. Observation of all the thorium−nitrogen−fluorides, however, inferred a possible reaction mechanism for the formation of ThNF starting from ThO_2 as shown below:

$$ThO_2 + 4NH_4HF_2 \xrightarrow{RT} (NH_4)_4ThF_8 + 2H_2O, \text{via} (NH_4)_3ThF_7$$

$$(NH_4)_4ThF_8 \xrightarrow{800°C,\ NH_3} ThF_4 + 4NH_4F$$

$$ThF_4 \xrightarrow{800°C,\ NH_3} ThN_{0.79}F_{1.63} \xrightarrow{800°C,\ NH_3} ThN_{0.9}F_{1.3} \xrightarrow{800°C,\ NH_3} ThNF$$

SEM imaging showed that the morphology of the samples involved in the reactions changed considerably. Plate-like morphology of the starting ThO_2 turned into an acicular particle shape upon conversion to $(NH_4)_4ThF_8$. The acicular $(NH_4)_4ThF_8$ particles became flat and agglomerated with partially crystallized facets upon thermal decomposition to ThF_4. Particles of ThNF produced by the ammonolysis of ThF_4 consist of plate-like particles with porous surfaces. The average particle size and shape of $(NH_4)_4ThF_8$ shown in the SEM image (Figure 3) are much different than that of the starting ThO_2, implying a difficulty in ThO_2 conversion to $(NH_4)_4ThF_8$ at room temperature. Formation of ThF_4, on the other hand, was reasonable based on the high gap in the crystalline character between $(NH_4)_4ThF_8$ and ThNF according to SEM imaging. Morphology of ThF_4 is at an intermediate position with respect to the change of acicular shape of $(NH_4)ThF_8$ to a thin plate-like particle shape of ThNF. The porous characteristics of the ThNF particles have relatively large surface areas. This increase is likely the explanation for ThNF reactions with minute oxygen content in the experimental setup. A longer exposure of ThNF to minute quantities of oxygen at elevated temperatures (i.e., 1100 °C) thus produces the ThO_2.

TEM also showed some prominent differences in the nanostrutures of $(NH_4)_4ThF_8$ and ThNF. Bulk area of the micro particles of $(NH_4)_4ThF_8$ exhibited polycrystalline characteristics with nanoscale crystalline patches. Some of these patches had fringe details in two directions while others showed fringe details either in one direction or none, showing the bulk of the particle to be low in crystallinity. Even in areas of high crystallinity, continuation of such crystallinity was disturbed by other polycrystalline characteristics. Therefore, the $(NH_4)_4ThF_8$ with its low-ordered crystal structure is vulnerable for attacks by other chemical agents and is easy to decompose into other compounds.

In the case of ThNF, most of the microparticle areas imaged showed well-oriented fringes with two-directional details, implying a high crystallinity. The porous characteristics identified from SEM imaging were also found at the nanoscale. Nanostructure of ThNF was easily observed with the HRTEM, and the crystal structure could also be confirmed. ThNF consisted of high-ordered nanostructure. Therefore, even at elevated temperatures it was difficult to change the chemical properties of the well-crystallized low-energy stable chemical phase. This is likely to contribute to the difficulty of removing further fluorine from ThNF to produce ThN_x. However, the overall thermodynamic favorability of the oxide phase may drive other crystalline chemical phases such as ThO_2.

5. Conclusion

Solid-state reaction of ThO_2 with NH_4HF_2 at room temperature formed two products: $(NH_4)_3ThF_7$ and $(NH_4)_4ThF_8$. The $(NH_4)_3ThF_7$ compound was produced quickly. The final product of the ammonolysis of $(NH_4)_4ThF_8$ at temperatures ranging from 800 to 1100 °C was found to be ThNF. Attempting to further react the material under NH_3, N_2, or N_2/H_2 (5%) to produce ThN_x chemical phases instead resulted in the formation of low-stoichiometric ThNF chemical phases with a minor ThO_2 phase. Formation of ThO_2 was most likely due to the trace oxygen in the experimental system, often formed at elevated temperatures over common laboratory equipment materials like the quartz used in this experiment. Thermal decomposition of $(NH_4)_4ThF_8$ to ThNF occurred through a ThF_4 intermediate and following a slow nitridization of ThF_4 under NH_3 through low-stoichiometric thorium−nitrogen−fluoride ternary chemical phases. Studies of the thermal behavior of ThNF under different chemical environments confirmed that the stoichiometric thorium nitrogen fluoride (ThNF) is the preferable chemical composition of all thorium nitride fluorides produced during the $(NH_4)_4ThF_8$ ammonolysis above 800 °C.

Distinct morphologies of the starting materials and final products of the reactions studied confirmed the chemical transformations identified by XRD. Polycrystalline characteristics were identified in the nanostructure of the $(NH_4)_4ThF_8$ where as in ThNF, long-ranged single crystal areas were observed over a wide range of the particles. Despite the appearance of the larger particles shown by SE SEM, HRTEM demonstrated the final ThNF product to be more crystalline than its precursors, thus explaining the high stability of ThNF toward substitution of fluorine with nitrogen.

Acknowledgment. The authors thank Dr. Anthony Hechanova for administrating the UNLV Transmutation Research Program under the financial support of the U.S. Department of Energy (Grant DE-FG07-01AL67358). We also thank Dr. Clay Crow from the Department of Geoscience and Dr. Longzhou Ma at UNLV, for helpful discussions and support. The authors are indebted to Tom O'Dou and Trevor Low for laboratory management and radiation safety.